



Article

Low-Cost Activated Grape Seed-Derived Hydrochar through Hydrothermal Carbonization and Chemical Activation for Sulfamethoxazole Adsorption

Elena Diaz *, Francisco Javier Manzano, John Villamil, Juan Jose Rodriguez and Angel F. Mohedano 

Chemical Engineering Department, Universidad Autonoma de Madrid, C/Francisco Tomás y Valiente 7, 28049 Madrid, Spain; francisco.manzano@uam.es (F.J.M.); john.villamil@uam.es (J.V.); juanjo.rodriguez@uam.es (J.J.R.); angelf.mohedano@uam.es (A.F.M.)

* Correspondence: elena.diaz@uam.es; Tel.: +34-914978035; Fax: +34-914973516

Received: 23 August 2019; Accepted: 23 November 2019; Published: 27 November 2019



Featured Application: Hydrothermal carbonization is presented as an alternative management way to valorize biomass wastes, and transform them in high-value solid products.

Abstract: Activated carbons were prepared by chemical activation with KOH, FeCl₃ and H₃PO₄ of the chars obtained via hydrothermal carbonization of grape seeds. The hydrochars prepared at temperatures higher than 200 °C yielded quite similar proximate and ultimate analyses. However, heating value (24.5–31.4 MJ·kg⁻¹) and energy density (1.04–1.33) significantly increased with carbonization temperatures between 180 and 300 °C. All the hydrochars showed negligible BET surface areas, while values between 100 and 845 m²·g⁻¹ were measured by CO₂ adsorption at 273 K. Activation of the hydrochars with KOH (activating agent to hydrochar ratio of 3:1 and 750 °C) led to highly porous carbons with around 2200 m²·g⁻¹ BET surface area. Significantly lower values were obtained with FeCl₃ (321–417 m²·g⁻¹) and H₃PO₄ (590–654 m²·g⁻¹), showing these last activated carbons important contributors to mesopores. The resulting materials were tested in the adsorption of sulfamethoxazole from aqueous solution. The adsorption capacity was determined by the porous texture rather than by the surface composition, and analyzed by FTIR and TPD. The adsorption equilibrium data (20 °C) fitted the Langmuir equation well. The KOH-activated carbons yielded fairly high saturation capacity reaching up to 650 mg·g⁻¹.

Keywords: grape seeds; hydrothermal carbonization; hydrochar; activated carbon; adsorption; sulfamethoxazole

1. Introduction

Biomass is a widely available source of energy, particularly important in developing countries, but cannot be considered a technically ideal fuel due to physical and chemical properties, each often having fibrous nature, high moisture content, volatile components, alkali and alkaline earth metallic content and a relatively low bulk density and heating value [1–3]. Thus, pre-treatment of biomass is in many cases convenient for efficient use as energy source. A broad range of biological (mainly anaerobic digestion and fermentation) and thermochemical (torrefaction and pyrolysis) treatments are typically used to improve the fuel properties of raw biomass [2,4,5]. From those processes, liquid or gaseous biofuels and even some valuable products are derived.

As an alternative to the classical thermochemical methods, hydrothermal carbonization (HTC), also referred to as wet torrefaction, is becoming an increasingly attractive way of biomass conversion. It operates in presence of water, at comparatively mild temperatures (180–300 °C) and a corresponding

saturation pressure [6–11]. The resulting solid product, usually called hydrochar (HC), is more stable and has higher carbon content than the starting substrate and improved (higher) heating value with respect to the char resulting from slow-pyrolysis or conventional carbonization at the same temperature [12–14]. In addition to the hydrochar, HTC gives rise to a high organic load aqueous stream [15,16], and a gas consisting mainly of CO₂.

Hydrochars have several industrial and environmental applications, such as for soil improvers [17] and solid fuel, whether upon direct combustion [18] or through gasification [12]. HTC chars may have also potential uses as sorbents for CO₂ sequestration, methane and hydrogen storage, in energy storage devices (Li/Na ion batteries, supercapacitors, fuel cells) and as precursors for activated carbon preparation [7,18–23].

In general, hydrochars show relatively low BET surface areas and pore volumes, which hinders their application as adsorbents [24]. Nevertheless, Titirici [23] reported the presence of ultramicropores (narrow micropores) in several sugar-derived hydrochars, as determined by CO₂ adsorption. Low-cost adsorbents can be obtained from HC upon further activation with different agents (CO₂, steam, acids, bases, or salts), allowing substantial pore volume and surface area increases, and even changes of the morphological structures of HTC chars [23–25]. A number of works have reported on the application of activated hydrochars in aqueous-phase adsorption for the removal of heavy metals [24,26–28], dyes [24,29], phenolic compounds [30] and emerging pollutants [18,31]. Gas-phase applications have been also studied, including, VOCs [32] and CO₂ [31,33] adsorption. Hydrochars treated by H₂O₂ oxidation have been used for lead removal from water [34].

Agricultural wastes are recognized as interesting feedstocks for inexpensive carbon materials [35]. Among them, grape seeds represent up to 15% of the solid wastes from the wine industry, where they are mostly burnt as fuel. Some papers have reported on the preparation of activated carbons by both physical and chemical activation from this precursor [36–40]. Activated carbon is widely available at low cost in many regions and its structural characteristics (granular morphology, size and preferential distribution of the lignocellulosic material in the periphery of the seed) make it particularly attractive for that purpose [36]. Essentially microporous activated carbons have been obtained by physical (CO₂) and chemical (KOH and K₂CO₃) activation [36,40]. Using phosphoric acid as the activating agent allowed obtaining also predominantly microporous carbons but with a broader porous texture with some significant contribution of mesoporosity [36]. Recently, Purnomo et al. [41] reported a two-stage process consisting of HTC followed by KOH-activation of the resulting hydrochar for the preparation of microporous carbons with high BET surface area under milder operating conditions than those used for direct single-step activation with the same agent.

The aim of this work was to study the valorization of grape seeds into carbon materials with the double purpose of obtaining high energy-density solid fuels upon hydrothermal carbonization and low-cost activated carbons by chemical activation of the resulting hydrochar. Temperature and biomass:water ratio have been analysed as operating conditions for HTC and KOH. FeCl₃ and H₃PO₄ have been tested as activating agents under different conditions. Hydrochars and activated carbons have been characterized by several techniques covering proximate and ultimate analyses, 77 K N₂ adsorption-desorption and CO₂ adsorption isotherms for porous texture, SEM for morphological examination and FTIR and TPD for surface functional groups assessment. Sulfamethoxazole, a sulfonamide antibiotic used to treat urinary infections was selected as the model compound to test the potential of the activated carbons as adsorbents for the removal of water pollutants. That compound is one of the most frequently emerging contaminants found in municipal wastewater, and in many cases is still present in the effluents from sewage treatment plants.

2. Materials and Methods

2.1. Preparation of Hydrochars

Grape seeds (GSs) provided by a local winery (“Tinta de Toro”, Zamora) were used as the hydrochar precursor. Table 1 shows the proximate and ultimate analyses. The HTC process was carried out in a Teflon-lined stainless steel vessel (100 mL), using 20 g of dried grape seeds and different water to GS ratios (10–60 wt.% of GSs). The reactor was sealed, inserted in a muffle furnace (Hobersal serie 8B Mod 12 PR/400, Hobersal, Barcelona, Spain) and heated up to 180–300 °C for 16 h. The hydrochar was recovered by filtration, washed with distilled water and oven-dried at 105 °C for 24 h (Nabertherm R 60/750/12-C6, Nabertherm, Bremen, Germany). The hydrochars were denoted as GS followed by the carbonization temperature and the dry GS percentage in the mixture. For instance, GS-260-40 represents the hydrochar obtained from grape seeds at 260 °C with 40% of dry GS. Table 1 includes also the hydrochar yield values calculated as the mass of the hydrochar per unit mass of GS, both on a dry basis.

Table 1. Proximate and ultimate analyses of grape seeds (GSs) and hydrochars (wt.% dry basis).

Sample	Yield (%)	Proximate Analysis (%)			Ultimate Analysis (%)				
		Volatile Matter	Fixed Carbon	Ash	C	H	N	S	O ¹
GS	-	73.3	24.3	2.4	56.5	6.6	1.8	0.13	32.6
GS-180-40	75	66.0	31.0	3.0	61.7	6.6	1.6	0.02	27.1
GS-200-40	77	59.2	37.6	3.2	63.8	6.4	1.7	0.01	24.9
GS-220-40	59	55.9	40.7	3.4	69.0	6.4	1.7	0.02	19.5
GS-240-40	59	55.2	41.6	3.2	69.2	6.2	2.0	0.02	19.4
GS-260-10	53	50.2	46.8	3.0	70.5	6.1	1.7	0.08	18.6
GS-260-20	62	49.8	46.6	3.6	70.9	6.4	1.8	0.04	17.3
GS-260-30	64	50.4	46.3	3.3	71.2	6.2	1.9	0.06	17.4
GS-260-40	63	50.3	46.4	3.3	70.7	6.3	1.9	0.05	17.8
GS-260-50	62	49.6	46.8	3.6	69.8	6.1	2.0	0.03	18.5
GS-260-60	64	50.6	45.9	3.5	70.0	6.2	2.1	0.02	18.1
GS-280-40	62	47.0	49.8	3.2	72.6	6.1	2.2	0.02	15.9
GS-300-40	48	43.8	51.8	4.4	74.0	5.8	2.3	0.01	13.5

¹ Calculated by difference O = 100 – (C + H + N + S + Ash).

The energy yield or energy recovery efficiency is calculated by [42] (also known as the energetic biomass utilization efficiency (BUE_E) [43]):

$$\text{Energy recovery efficiency} = \text{Hydrochar yield} \cdot \text{Energy density},$$

where the energy density is the ratio of the higher heating values of the char relative to that of the grape seeds.

2.2. Preparation of Activated Carbons

The activated carbons (ACs) were prepared using either potassium hydroxide (KOH), iron chloride (FeCl₃) or phosphoric acid (H₃PO₄), which were physically mixed with the ground hydrochar at different activating agent to HC ratios of 4:1, 3:1 and 2:1 (w:w). In the case of H₃PO₄, the mixture was left overnight at 60 °C and then heated at 500 °C for 2 h under continuous N₂ flow (100 NmL·min⁻¹) in a stainless steel tube placed in an electrical furnace. The activation temperature was reached at 10 °C·min⁻¹ heating rate. Activation with KOH and FeCl₃ was performed similarly but at 750 °C for 1 h [44–47]. After cooling under nitrogen flow, the ACs were washed with HCl or NaOH 0.1 M until neutral pH; then were washed with distilled water; and finally, were dried at 105 °C overnight. The ACs were denoted as GSHC, followed by the activating agent and the activating agent:hydrochar (w:w) ratio. For instance, GSHC-KOH-3 represents the activated carbon obtained with KOH using 3:1 activating agent to hydrochar ratio.

2.3. Characterization of Hydrochar and Activated Carbons

The proximate analyses were performed by the ASTM methods D3173-11 (moisture), D3174-11 (ash) and D3175-11 (volatile matter (VM)) using a Mettler Toledo apparatus (TGA/SDTA851e). The elemental analyses were carried out in a LECO Model CHNS-932 elemental analyzer. The higher heating value (HHV) of hydrochar samples was determined using an IKA Calorimeter System C2000 according to the ASTM D5865 procedure.

The porous texture of the AC samples was characterized by 77 K N₂ adsorption-desorption in a Micromeritics apparatus (Tristar 3020, Micromeritics, Narcross, GA, USA). The samples were previously degassed (150 °C for 6 h) in a Micromeritics VacPrep 061 device (Micromeritics, Narcross, GA, USA). The surface area was calculated by the BET equation within the 0.05–0.30 relative pressure range and the micropore volume (V_{micro}) was obtained by the t-method. The difference between the volume of N₂ adsorbed at 0.95 relative pressure (as liquid) and the micropore volume was taken as the mesopore volume (V_{meso}). The external or non-micropore surface area (A_{ext}) was also obtained from the t method. Surface area and micropore volume of the samples were also determined by CO₂ adsorption at 273 K in the same equipment. The corresponding surface area (S_{DA}) and the micropore volume ($V_{\text{micro-DA}}$) values were calculated by the Dubinin–Astakhov equation [48].

The surface composition of the hydrochars and activated carbons was analyzed by FTIR spectroscopy using a FTIR Bruker IFS66v spectrophotometer (Bruker Corporation, Billerica, MA, USA), with a KBr disc, having a resolution of 4 cm⁻¹ from 4000 to 550 cm⁻¹ and 250 scans. Temperature programmed desorption (TPD) was also used to assess the amount of oxygen surface groups. The samples (0.1 g) were heated up to 900 °C at 10 °C·min⁻¹ in a vertical quartz tube under continuous N₂ flow of 1 NL·min⁻¹. The amounts of CO₂ and CO evolved were analyzed by non-dispersive infrared absorption in a Siemens model Ultramat 22 equipment (Siemens Aktiengesellschaft, Munich, Germany).

The morphologies of hydrochars and activated carbon samples were studied by scanning electron microscopy (SEM) with a Hitachi S-3000N apparatus (Hitachi Ltd, Tokyo, Japan). The samples were metalized with gold using a Sputter Coater SC502 (Quorum, East Sussex, UK). Images were obtained in the high vacuum mode under an accelerating voltage of 20 kV, using secondary and backscattered electrons.

The pH slurry of the carbons was determined measuring the pH (pH-meter, Crison) of an aqueous suspension of the sample (1 g) in distilled water (10 mL) [49].

2.4. Adsorption Tests

The potential application of the activated carbons as adsorbents in aqueous phase was evaluated using sulfamethoxazole (SMX) as model impurity, which has a solubility in water of 610 mg·L⁻¹ at 298 K. Samples of AC (12.5 mg, ≈100 μm) were contacted in stoppered glass bottles with 50 mL of SMX aqueous solutions (25 to 150 mg·L⁻¹). A commercial activated carbon (C: 89.5 wt.%, A_{BET} : 800 m²·g⁻¹; V_{micro} : 0.67 cm³·g⁻¹; V_{meso} : 0.53 cm³·g⁻¹), supplied by Merck, was also used as reference for comparison purposes. Experiments were carried out at 20 °C and the natural pH of the SMX solution (4.6) in a thermostated shaker (Optic Ivymen System, Biotech, Madrid, Spain) at equivalent 200 rpm. A kinetic experiment showed that 5 days was time enough to reach the adsorption equilibrium in the operating conditions. SMX concentration was determined by UV–vis spectrophotometry (Cary 60 UV-Vis, Agilent Technologies, Santa Clara, CA, USA) at 265 nm wavelength. The Langmuir equation was used to fit the equilibrium data. The reported results are the average values from triplicate runs, being the standard errors always below 5%.

3. Results and Discussion

3.1. Characterization of the Hydrochars

Table 1 shows the hydrochar yields and the proximate and ultimate analyses of the raw GSs and hydrochars. Hydrochar yields were almost constant (≈60–65 wt.%) in the HTC runs performed with

a GS relative amount higher than 20% in the GS + water mixture within the temperature range of 220–280 °C (aprox.). At a lower GS percentage the HC yield decreased since a higher relative amount of water favors the extraction and transfer of solid components to the liquid phase [12,50]. The effect of the temperature in the HTC process can be seen at fixed GS percentage in the starting mixture (40 wt.%) and temperatures below and above the aforementioned range. At temperatures ≤ 200 °C, high HC yields were obtained associated to lower carbonization as can be seen from the C content of the samples. At temperature above 280 °C gasification reactions gain significance, giving rise to lower yield but a more carbonized solid [51]. It is well known that dehydration and decarboxylation reactions are the main responsible of the mass loss upon HTC [52,53].

A van Krevelen diagram was plotted from the ultimate analyses (Figure 1) where the points corresponding to the HCs have been placed. As the HTC temperature increases, the resulting HCs evolve from a typical peat composition towards the lignite region, approaching even sub-bituminous coal at the highest HTC temperature tested (300 °C).

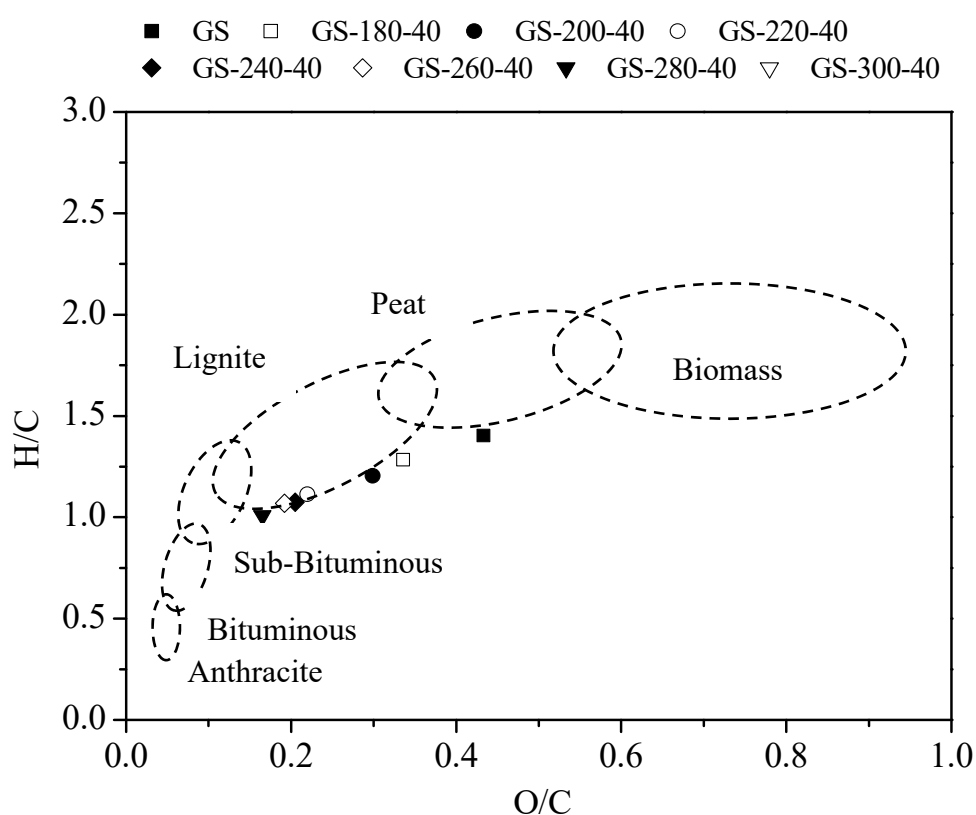


Figure 1. Van Krevelen diagram for grape seeds and hydrochars obtained at different temperatures (180–300 °C) with an initial solid content of 40 wt.%.

Table 2 summarizes the energy properties of hydrochars, where, clearly, there was a significant increase of the higher heating value as the HTC temperature increased. The energy density of the most carbonized solid was improved by one-third with respect to the starting precursor. Taking into account the GS to HC yield, the highest energy recovery efficiency does not correspond to the highest HTC temperature tested but to a significantly lower value somewhere around 200 °C. However, since the energy density of the resulting fuel is also an important issue, the information provided by Table 2 points to an optimum HTC temperature in the range of 260–280 °C. Moreover, this determination, also known as a BUE_E , provides an extra information because it allows a comparison between different fuels and options for biomass utilization [43].

Table 2. Energy properties of raw grape seeds and hydrochars.

Sample	HHV (MJ·kg ⁻¹)	Energy Density	Energy Recovery Efficiency ¹
GS	23.6	-	-
GS-180-40	24.5	1.04	0.78
GS-200-40	26.8	1.14	0.87
GS-220-40	27.6	1.17	0.69
GS-240-40	29.1	1.23	0.73
GS-260-40	30.3	1.29	0.81
GS-280-40	30.9	1.31	0.81
GS-300-40	31.4	1.33	0.64

¹ Also known as BUE_E.

The 77 K N₂ adsorption isotherms of the hydrochars (supporting material) corresponded to Type II of the IUPAC classification, associated to non-porous solids. The highest BET surface area was only 8 m²·g⁻¹, corresponding to the GS-220-40 sample. To learn more on the porous texture of these hydrochars the CO₂ adsorption isotherms at 273 K were obtained (Supplementary Material). The surface area values from those isotherms (S_{DA}) varied from 100 to 845 m²·g⁻¹, the highest corresponding to the above mentioned sample, with a micropore volume of 0.513 cm³·g⁻¹. These huge differences between the BET and S_{DA} values are indicative of microporous texture consisting essentially of very narrow micropores, the so-called ultramicropores (≤0.5 nm width), corresponding most probably to slit-shaped pores. This type of microporosity has been also observed in chars from HTC of different sugars at 180 °C calcined at high temperatures in an inert atmosphere [23].

3.2. Activated Carbons by Chemical Activation of Hydrochars

Previous works have proven that hydrochars can be more effective adsorbents than thermal (pyrolytic) biochars due to their diverse structures and surface functional groups [54]. Looking at the characteristics of the hydrochars, the GS-220-40 was selected for further activation to achieve a well-developed porosity typical of a carbon-based adsorbent. In previous works [23] HTCs obtained at 180–240 °C were more prone to yield a better developed porosity upon KOH-activation than those obtained above 260 °C, although from fairly different precursors than in the current work.

Table 3 summarizes the porous textures of the activated carbons. Representative N₂ adsorption-desorption isotherms are depicted in Figure 2. All of them correspond to essentially microporous solids; there was a higher contribution of mesoporosity in the case of H₃PO₄-activation. The rest of isotherms are given as Supplementary Material (Figures S1–S3). KOH was by far the activating agent allowing the highest porosity development, with BET surface area values up to ca. 2200 m²·g⁻¹. These carbons were essentially microporous with increased mesoporosity at increasing KOH to hydrochar mass ratio. The activated carbon prepared at 4:1 mass ratio had almost 1800 m²·g⁻¹ BET surface area in spite of its high ash content (38.2%), mostly due to the remaining inorganic matter derived from the activating agent. In fact, its BET surface area represented as much as ca. 2900 m²·g⁻¹ on an ash-free basis.

The lowest surface area development occurred with FeCl₃ as activating agent, due in part to the very high ash content of the resulting activated carbons. The highest BET surface area of these carbons on an ash-free basis was 770 m²·g⁻¹, only slightly more than one-quarter that of the abovementioned KOH-activated carbon. FeCl₃-activation can be addressed to the preparation of carbon-supported Fe catalysts. Bedia et al. [44] and Mena et al. [55] prepared this type of catalyst, and tested theirs in catalytic wet peroxide oxidation (CWPO), from FeCl₃-activation of sewage sludge.

Activation with H₃PO₄ gave rise to microporous carbons but with much higher relative contribution of mesoporosity, showing Type IV isotherms of the IUPAC classification. The BET surface area values are relatively low compared to the obtained by the same method with other precursors. The ash content was significantly lower than by the two other activation procedures. Increasing the H₃PO₄ to HC ratio decreased the BET surface area, affecting mostly, the mesopore contribution.

Table 3. Textural characteristics of the activated carbons.

Sample	C (wt.% Dry Basis)	Ash (wt.% Dry Basis)	A _{BET} (m ² ·g ⁻¹)	A _{ext} (m ² ·g ⁻¹)	V _{micro} (cm ³ ·g ⁻¹)	V _{meso} (cm ³ ·g ⁻¹)
GSHC-KOH-2	75.1	9.8	1215	35	0.57	0.02
GSHC-KOH-3	73.3	16.3	2194	121	0.98	0.05
GSHC-KOH-4	45.6	38.2	1780	260	0.74	0.18
GSHC-FeCl ₃ -2	51.1	44.4	394	44	0.17	0.02
GSHC-FeCl ₃ -3	49.7	46.0	417	54	0.17	0.02
GSHC-FeCl ₃ -4	35.7	49.2	312	50	0.12	0.02
GSHC-H ₃ PO ₄ -2	63.3	4.6	654	255	0.19	0.23
GSHC-H ₃ PO ₄ -3	61.4	7.6	596	242	0.17	0.21
GSHC-H ₃ PO ₄ -4	69.7	10.8	590	172	0.20	0.16

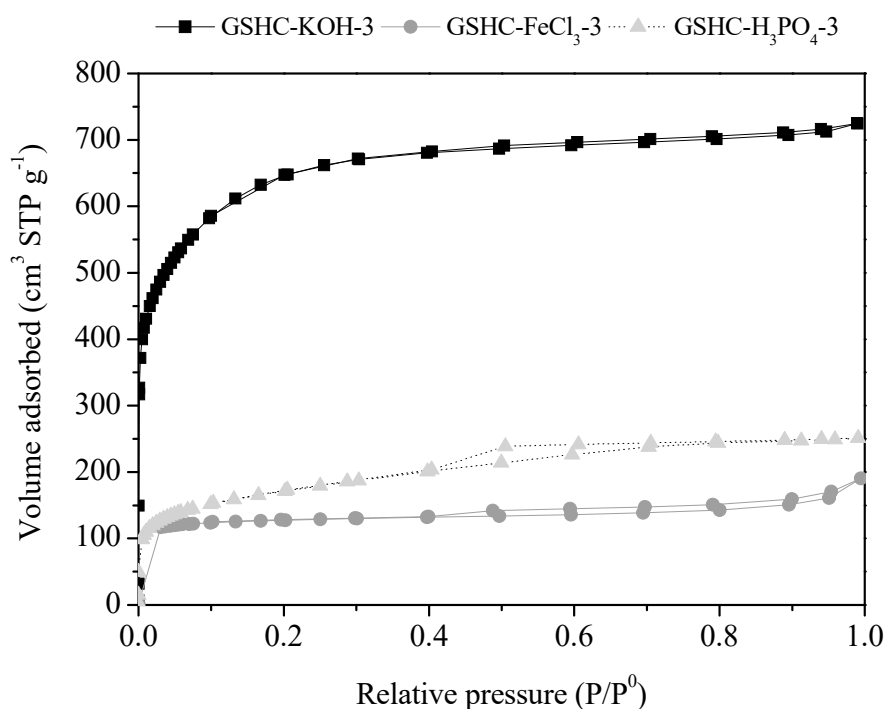


Figure 2. N₂ adsorption-desorption isotherms at 77 K of the activated carbons obtained at 3:1 activating agent to hydrochar ratio.

Figure 3 shows SEM images of the grape seeds, hydrochars and activated carbons. The raw GSs exhibited a well-defined morphological structure in three different layers, while in the hydrochar image shows some partial degradation of the structure occurred, although the morphology was still preserved in great part, which indicates good thermomechanical stability for the GSs. This allows obtaining granular activating carbons from this starting material. KOH activation produced a spongy-like structure with many holes. In the case of FeCl₃-activation, the formation of microspheres was visible; after the activation with H₃PO₄, prismatic particles can be seen.

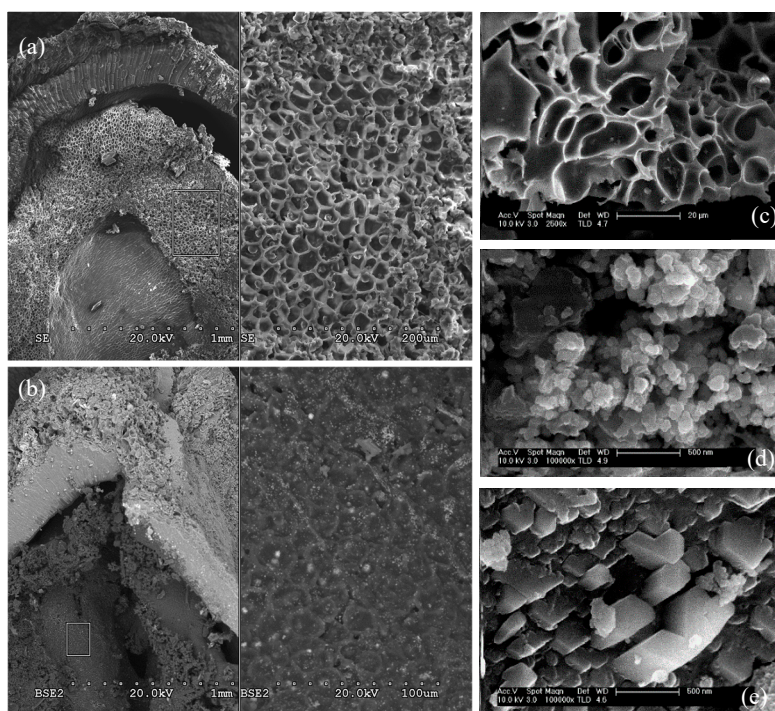


Figure 3. SEM images of cross-section of GS (a), GS-220-40 hydrochar (b), and GSAC-KOH-3 (c), GSAC-FeCl₃-3 (d) and GSAC-H₃PO₄-3 (e) activated carbons.

Figure 4 shows the FTIR spectra of the raw GS, GS-220-40 hydrochar and the activated carbons obtained with an activating agent to hydrochar ratio of 3. A decreasing intensity of the O–H stretching of the hydroxyl groups at 3400 cm^{−1} was observed for the hydrochar, because the dehydration occurred upon HTC [56,57]. The bands appearing in the 2950 to 2750 cm^{−1} range, associated to aliphatic carbon –CH_x stretching vibration, tended to be less intense for the GS-220-40 hydrochar, probably due to the evolution of nonpolar alkyl carbon structure [58]. In addition, transmission intensities at 1750–750 cm^{−1} arising from C=O stretching of ketones and other carbonyl structures were reduced. Furthermore, the decline of the peak at 1030 cm^{−1} (the C–O and C–O–C stretching) indicates that both decarboxylation and dehydration occur, consistently with the van Krevelen representation of Figure 1.

The FTIR spectra of activated carbons showed a dramatic decrease of functionalities in agreement with the reported in general in the literature relative to activation of carbon precursors. A broad band (3600–3100 cm^{−1}) appears in the three activated carbons, related to the existence of hydroxyl functional groups. Those related to C=C and aromatic rings vibration (1600–1500 cm^{−1}) and the associated to C–O bonds at 1157–1090 cm^{−1}, related to the presence of alcohol groups were more intense in the GSHC-FeCl₃-3, and, mainly, in the GS-H₃PO₄-3 activated carbons [59,60].

The amount of surface oxygen groups in the activated carbons was assessed in terms of CO₂ and CO evolved upon TPD. The results are summarized in the inside Table of Figure 4. In all the cases, the ratio CO₂/CO was within 27–30%, suggesting that the oxygen groups must be ascribed majorly to CO-evolving functionalities (phenol, carbonyl, anhydride ether, quinone), mainly associated to weak acid and neutral/basic surfaces. However, there are also some significant amounts of evolved CO₂, such that carboxylic, lactone and anhydride groups may be also present in some extent [61,62]. H₃PO₄, and in particular, FeCl₃, appear to be more prone than KOH to create oxygen groups on the carbon surface upon activation. Rey et al. [62] arrived to similar conclusion working with Fe(NO₃)₃ as a precursor.

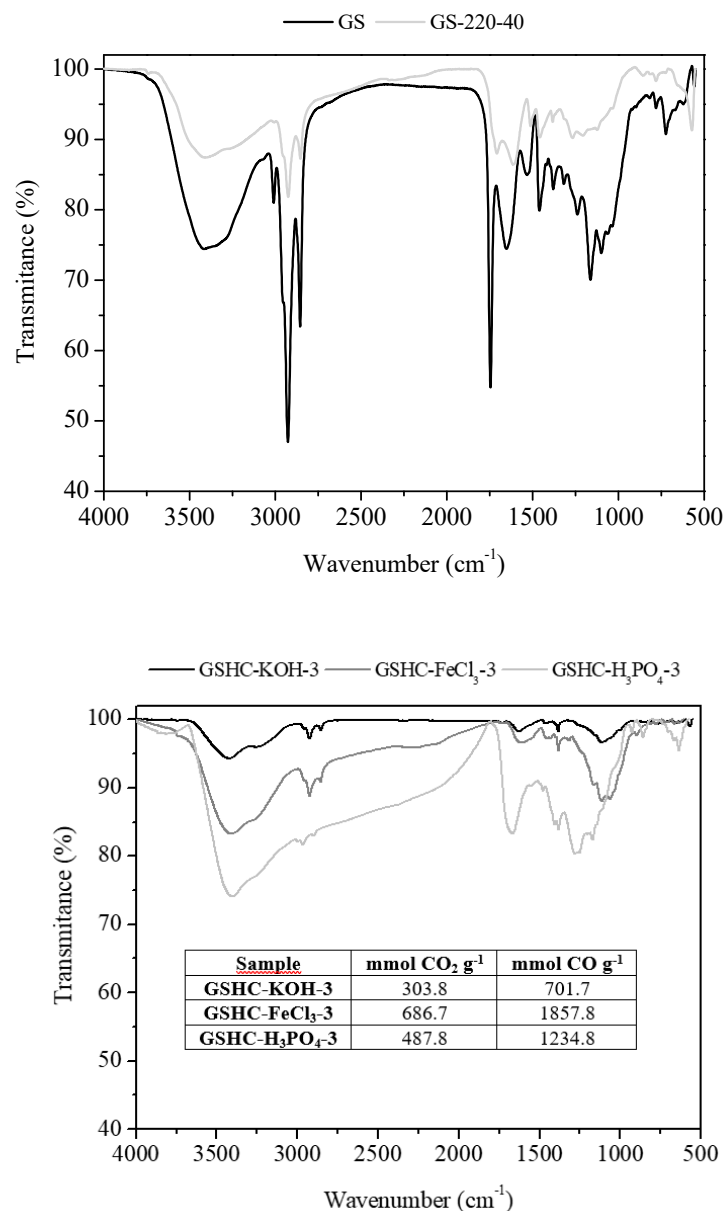


Figure 4. FTIR spectra for GS, GS-220-40 hydrochar and activated carbons. Results of TPD of the activated carbons in the inside Table.

3.3. Adsorption of Sulfamethoxazole

Figure 5 shows the adsorption isotherms (20 °C) of SMX with the GSAC-KOH-3, GSAC-FeCl₃-3 and GSAC-H₃PO₄-3 activated carbons and a commercial active carbon. The adsorption capacity seems to be mainly determined by the BET surface area of the carbons rather than the amount and character of the surface groups (Figure 4). Consistently with its much higher surface area, GSHC-KOH-3 yielded the highest adsorption capacity. The only deviation of that behavior occurred with the GSHC-H₃PO₄-3 activated carbon, which showed lower adsorption than the expected from its BET surface area. This can be explained in terms of SMX ionization and the pH slurry of this carbon. At solution pH 4.6, SMX (pKa1: 1.7, pKa2: 5.6 [63]) must be majorly made of neutral and anion species; since the pH slurry of GSHC-H₃PO₄-3 is 2.2, its surface will be negatively charged, which induces repulsion forces between the molecules of SMX and the carbon surface [64,65].

The experimental data were fitted to the Langmuir equation:

$$q_e = \frac{q_L \cdot K_L \cdot C_e}{1 + K_L \cdot C_e}$$

where q_e is the equilibrium adsorbate loading onto the adsorbent ($\text{mg}\cdot\text{g}^{-1}$), C_e the equilibrium liquid-phase concentration of the adsorbate ($\text{mg}\cdot\text{L}^{-1}$), q_L the monolayer saturation capacity ($\text{mg}\cdot\text{g}^{-1}$) and K_L the Langmuir constant ($\text{L}\cdot\text{mg}^{-1}$). This equation described the equilibrium data well, as can be seen in Figure 5. The values of the fitting parameters and the correlation coefficients are given in Table 4. The calculated monolayer Langmuir capacity of GSHC-KOH-3 reached $650 \text{ mg}\cdot\text{g}^{-1}$ (notice that in Figure 5 the represented experimental SMX values did not reach the saturation level). The SMX adsorption capacity of this material is higher than the exhibited by other adsorbents, such as activated carbon from pine tree or coconut shell, coal, carbon nanotubes, graphene and organo-montmorillonites at similar operating conditions, which are characterized by maximum adsorption capacities within the range of $122\text{--}242 \text{ mg}\cdot\text{g}^{-1}$ [65–67].

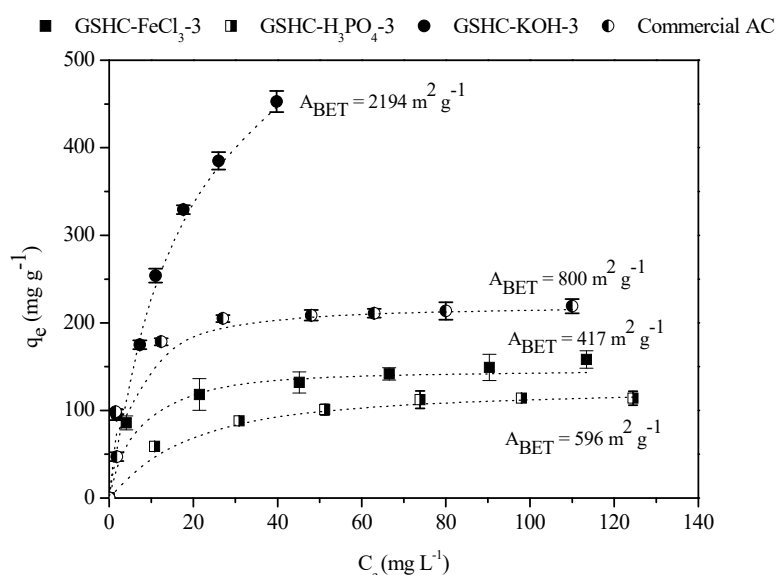


Figure 5. Adsorption isotherms of SMX on GSHC-KOH-3, GSHC-FeCl₃-3, GSHC-H₃PO₄-3 and commercial activated carbon at 20 °C (symbols: experimental values; short dot lines: fitting to the Langmuir equation). Error bars are included.

Table 4. Langmuir parameters for SMX adsorption on the activated carbons of Figure 5.

Sample	pH Slurry	q_L ($\text{mg}\cdot\text{g}^{-1}$)	K_L ($\text{L}\cdot\text{mg}^{-1}$)	R^2
GSHC-KOH-3	7.6	650.8	0.055	0.983
GSHC-FeCl ₃ -3	8.1	147.4	0.295	0.963
GSHC-H ₃ PO ₄ -3	2.2	128.6	0.069	0.988
Commercial AC	7.7	221.8	0.296	0.951

4. Conclusions

Hydrothermal carbonization of grape seeds is a promising way of valorization of that biomass waste from the wine industry. It allows obtaining chars of fairly good properties to be used as improved solid fuel. Further activation of those chars leads to higher value-added products, activated carbons. Activation with FeCl₃, H₃PO₄ and KOH led to high BET surface area carbons of predominantly microporous texture, which can be useful adsorbents for liquid-phase applications, as in water pollutant

removal. In fact, a fairly high adsorption capacity was experimentally found with sulfamethoxazole, an emerging contaminant, as the target compound.

Supplementary Materials: The following are available online at <http://www.mdpi.com/2076-3417/9/23/5127/s1>: Figure S1: N₂ adsorption-desorption isotherms at 77 K of hydrochars, Figure S2: CO₂ adsorption isotherms at 273 K of hydrochars, Figure S3: N₂ adsorption-desorption isotherms at 77 K of activated carbons not included in Figure 2.

Author Contributions: Conceptualization, E.D., J.J.R. and A.F.M.; methodology, E.D., F.J.M. and J.V.; investigation, E.D., F.J.M. and J.V.; writing—original draft preparation, E.D. and F.J.M.; writing—review and editing, E.D., J.J.R. and A.F.M.; supervision, J.V., J.J.R. and A.F.M.; funding acquisition, E.D., J.J.R. and A.F.M.

Funding: The authors greatly appreciate financial support from the Spanish MINECO (CTM2016-76564-R), Comunidad de Madrid (S2018/EMT-4344) and UAM-Santander (2017/EEUU/07). F.J. Manzano wishes to thank the Comunidad de Madrid (PEJ16/AMB/AI-1327) for a research grant.

Conflicts of Interest: The authors declare no conflict of interest.

References

1. Demirbas, A. Combustion characteristics of different biomass fuels. *Prog. Energy Combust. Sci.* **2004**, *30*, 219–230. [CrossRef]
2. Goyal, H.B.; Seal, D.; Saxena, R.C. Biofuels from thermochemical conversion of renewable resources: A review. *Renew. Sustain. Energy Rev.* **2008**, *12*, 504–517. [CrossRef]
3. Yip, K.; Tian, F.; Hayashi, J.-I.; Wu, H. Effect of alkali and alkaline earth metallic species on biochar reactivity and syngas compositions during steam gasification. *Energy Fuel.* **2009**, *24*, 173–181. [CrossRef]
4. Saxena, R.; Adhikari, D.; Goyal, H. Biomass-based energy fuel through biochemical routes: A review. *Renew. Sustain. Energy Rev.* **2009**, *13*, 167–178. [CrossRef]
5. Kambo, H.S.; Dutta, A. A comparative review of biochar and hydrochar in terms of production, physico-chemical properties and applications. *Renew. Sustain. Energy Rev.* **2015**, *45*, 359–378. [CrossRef]
6. Berge, N.D.; Ro, K.S.; Mao, J.; Flora, J.R.V.; Chappell, M.A.; Bae, S. Hydrothermal carbonization of municipal waste streams. *Environ. Sci. Technol.* **2011**, *45*, 5696–5703. [CrossRef]
7. Falco, C.; Marco-Lozar, J.P.; Salinas-Torres, D.; Morallón, E.; Cazorla-Amorós, D.; Titirici, M.M.; Lozano-Castelló, D. Tailoring the porosity of chemically activated hydrothermal carbons: Influence of the precursor and hydrothermal carbonization temperature. *Carbon* **2013**, *62*, 346–355. [CrossRef]
8. Funke, A.; Ziegler, F. Hydrothermal carbonization of biomass: A summary and discussion of chemical mechanisms for process engineering. *Biofuels Bioprod. Biorefin.* **2010**, *4*, 160–177. [CrossRef]
9. Hitzl, M.; Corma, A.; Pomares, F.; Renz, M. The hydrothermal carbonization (HTC) plant as a decentral biorefinery for wet biomass. *Catal. Today* **2015**, *257*, 154–159. [CrossRef]
10. Hrnčič, M.K.; Kravanja, G.; Knez, Ž. Hydrothermal treatment of biomass for energy and chemicals. *Energy* **2016**, *116*, 1312–1322. [CrossRef]
11. Sermyagina, E.; Saari, J.; Kaikko, J.; Vakkilainen, E. Hydrothermal carbonization of coniferous biomass: Effect of process parameters on mass and energy yields. *J. Anal. Appl. Pyrolysis* **2015**, *113*, 551–556. [CrossRef]
12. Álvarez-Murillo, A.; Román, S.; Ledesma, B.; Sabio, E. Study of variables in energy densification of olive stone by hydrothermal carbonization. *J. Anal. Appl. Pyrolysis* **2015**, *113*, 307–314. [CrossRef]
13. Román, S.; Nabais, J.M.V.; Laginhas, C.; Ledesma, B.; González, J.F. Hydrothermal carbonization as an effective way of densifying the energy content of biomass. *Fuel Process. Technol.* **2012**, *103*, 78–83. [CrossRef]
14. Wüst, D.; Rodríguez Correa, C.; Suwelack, K.U.; Köhler, H.; Kruse, A. Hydrothermal carbonization of dry toilet residues as an added-value strategy—Investigation of process parameters. *J. Environ. Manag.* **2019**, *234*, 537–545. [CrossRef]
15. De la Rubia, M.A.; Villamil, J.A.; Rodríguez, J.J.; Mohedano, A.F. Effect of inoculum source and initial concentration on the anaerobic digestion of the liquid fraction from hydrothermal carbonisation of sewage sludge. *Renew. Energy* **2018**, *127*, 697–704. [CrossRef]
16. Villamil, J.A.; Mohedano, A.F.; Rodríguez, J.J.; De la Rubia, M.A. Anaerobic co-digestion of the aqueous phase from hydrothermally treated waste activated sludge with primary sewage sludge. *J. Environ. Manag.* **2019**, *231*, 726–733. [CrossRef]

17. Bargmann, I.; Rillig, M.C.; Kruse, A.; Greef, J.-M.; Kücke, M. Effects of hydrochar application on the dynamics of soluble nitrogen in soils and on plant availability. *J. Plant Nutr. Soil Sci.* **2014**, *177*, 48–58. [[CrossRef](#)]
18. Fernandez, M.E.; Ledesma, B.; Román, S.; Bonelli, P.R.; Cukierman, A.L. Development and characterization of activated hydrochars from orange peels as potential adsorbents for emerging organic contaminants. *Bioresour. Technol.* **2015**, *183*, 221–228. [[CrossRef](#)]
19. Guo, S.; Dong, X.; Wu, T.; Zhu, C. Influence of reaction conditions and feedstock on hydrochar properties. *Energy Convers. Manag.* **2016**, *123*, 95–103. [[CrossRef](#)]
20. Fang, J.; Zhan, L.; Ok, Y.S.; Gao, B. Minireview of potential applications of hydrochar derived from hydrothermal carbonization of biomass. *J. Ind. Eng. Chem.* **2018**, *57*, 15–21. [[CrossRef](#)]
21. Heidari, M.; Dutta, A.; Acharya, B.; Mahmud, S. A review of the current knowledge and challenges of hydrothermal carbonization for biomass conversion. *J. Energy Inst.* **2019**, *92*, 1779–1799. [[CrossRef](#)]
22. Nizamuddin, S.; Baloch, H.A.; Griffin, G.J.; Mubarak, N.M.; Bhutto, A.W.; Abro, R.; Mazari, S.A.; Ali, B.S. An overview of effect of process parameters on hydrothermal carbonization of biomass. *Renew. Sustain. Energy Rev.* **2017**, *73*, 1289–1299. [[CrossRef](#)]
23. Titirici, M.M. Hydrothermal Carbons: Synthesis, Characterization, and Applications. In *Novel Carbon Adsorbents*, 1st ed.; Tascón, J.M.D., Ed.; Elsevier Ltd.: Oxford, UK, 2012; pp. 351–399.
24. Fang, J.; Gao, B.; Zimmerman, A.R.; Ro, K.S.; Chen, J.J. Physically (CO₂) activated hydrochars from hickory and peanut hull: Preparation, characterization, and sorption of methylene blue, lead, copper, and cadmium. *RSC Adv.* **2016**, *6*, 24906–24911. [[CrossRef](#)]
25. Wang, B.; Gao, B.; Fang, J. Recent advances in engineered biochar productions and applications. *Crit. Rev. Environ. Sci. Technol.* **2017**, *47*, 2158–2207. [[CrossRef](#)]
26. Aliakbari, Z.; Younesi, H.; Ghoreyshi, A.A.; Bahramifar, N.; Heidari, A. Sewage sludge-based activated carbon: Its application for hexavalent chromium from synthetic and electroplating wastewater in batch and fixed-bed column adsorption. *Desalin. Water Treat.* **2017**, *93*, 61–73. [[CrossRef](#)]
27. Regmi, P.; Moscoso, J.L.G.; Kumar, S.; Cao, X.; Maob, J.; Schafran, G. Removal of copper and cadmium from aqueous solution using switchgrass biochar produced via hydrothermal carbonization process. *J. Environ. Manag.* **2012**, *109*, 61–69. [[CrossRef](#)]
28. Zhang, X.; Zhang, L.; Li, A. Eucalyptus sawdust derived biochar generated by combining the hydrothermal carbonization and low concentration KOH modification for hexavalent chromium removal. *J. Environ. Manag.* **2018**, *206*, 989–998. [[CrossRef](#)]
29. Islam, A.; Ahmed, M.J.; Khanday, W.A.; Asif, M.; Hameed, B.H. Mesoporous activated coconut shell-derived hydrochar prepared via hydrothermal carbonization-NaOH activation for methylene blue adsorption. *J. Environ. Manag.* **2017**, *203*, 237–244. [[CrossRef](#)]
30. Jain, A.; Balasubramanian, R.; Srinivasan, M.P. Tuning hydrochar properties for enhanced mesopore development in activated carbon by hydrothermal carbonization. *Microporous Mesoporous Mater.* **2015**, *203*, 178–185. [[CrossRef](#)]
31. Puccini, M.; Stefanelli, E.; Tasca, A.L.; Vitolo, S. Pollutant Removal from gaseous and aqueous phases using hydrochar-based activated carbon. *Chem. Eng. Trans.* **2018**, *67*, 637–642.
32. Zhang, X.; Gao, B.; Fang, J.; Zou, W.; Dong, L.; Cao, C.; Zhang, J.; Li, Y.; Wang, H. Chemically activated hydrochar as an effective adsorbent for volatile organic compounds (VOCs). *Chemosphere* **2019**, *218*, 680–686. [[CrossRef](#)]
33. Rodríguez-Correa, C.; Bernardo, M.; Ribeiro, R.P.P.L.; Esteves, I.A.A.C.; Kruse, A. Evaluation of hydrothermal carbonization as a preliminary step for the production of functional materials from biogas digestate. *J. Anal. Appl. Pyrolysis* **2017**, *124*, 461–474. [[CrossRef](#)]
34. Xue, Y.; Gao, B.; Yao, Y.; Inyang, M.; Zhang, M.; Zimmerman, A.R.; Ro, K.S. Hydrogen peroxide modification enhances the ability of biochar (hydrochar) produced from hydrothermal carbonization of peanut hull to remove aqueous heavy metals: Batch and column tests. *Chem. Eng. J.* **2012**, *200*, 673–680. [[CrossRef](#)]
35. Zhang, T.; Wu, X.; Fan, X.; Tsang, D.C.W.; Li, G.; Shen, Y. Corn waste valorization to generate activated hydrochar to recover ammonium nitrogen from compost leachate by hydrothermal assisted pretreatment. *J. Environ. Manag.* **2019**, *236*, 108–117. [[CrossRef](#)]
36. Al Bahri, M.; Calvo, L.; Gilarranz, M.A.; Rodríguez, J.J. Activated carbon from grape seeds upon chemical activation with phosphoric acid: Application to the adsorption of diuron from water. *Chem. Eng. J.* **2012**, *203*, 348–356. [[CrossRef](#)]

37. Al Bahri, M.; Calvo, L.; Gilarranz, M.A.; Rodriguez, J.J. Diuron multilayer adsorption on activated carbon from CO₂ activation of grape seeds. *Chem. Eng. Commun.* **2016**, *203*, 103–113. [[CrossRef](#)]
38. Jimenez-Cordero, D.; Heras, F.; Alonso-Morales, N.; Gilarranz, M.A.; Rodriguez, J.J. Porous structure and morphology of granular chars from flash and conventional pyrolysis of grape seeds. *Biomass Bioenergy* **2013**, *54*, 123–132. [[CrossRef](#)]
39. Jimenez-Cordero, D.; Heras, F.; Gilarranz, M.A.; Raymundo-Piñero, E. Grape seed carbons for studying the influence of texture on supercapacitor behaviour in aqueous electrolytes. *Carbon* **2014**, *71*, 27–138. [[CrossRef](#)]
40. Okman, I.; Karagöz, S.; Tay, T.; Erdem, M. Activated carbons from grape seeds by chemical activation with potassium carbonate and potassium hydroxide. *Appl. Surf. Sci.* **2014**, *293*, 138–142. [[CrossRef](#)]
41. Purnomo, C.; Castello, D.; Fiori, L. Granular activated carbon from grape seeds hydrothermal char. *Appl. Sci.* **2018**, *8*, 331. [[CrossRef](#)]
42. Park, K.Y.; Lee, K.; Kim, D. Characterized hydrochar of algal biomass for producing solid fuel through hydrothermal carbonization. *Bioresour. Technol.* **2018**, *258*, 119–124. [[CrossRef](#)]
43. Iffland, K.; Sherwood, J.; Carus, M.; Raschka, A.; Farmer, T.; Clark, J. Calculation and Comparison of the “Biomass Utilization Efficiency (BUE)” of Various Bio-based Chemicals, Polymers and Fuels. Available online: http://bio-based.eu/?did=32321&vp_edd_act=show_download (accessed on 5 September 2019).
44. Bedia, J.; Monsalvo, V.M.; Rodriguez, J.J.; Mohedano, A.F. Iron catalysts by chemical activation of sewage sludge with FeCl₃ for CWPO. *Chem. Eng. J.* **2017**, *318*, 224–230. [[CrossRef](#)]
45. Bedia, J.; Belver, C.; Ponce, S.; Rodriguez, J.; Rodriguez, J.J. Adsorption of antipyrine by activated carbons from FeCl₃-activation of Tara gum. *Chem. Eng. J.* **2018**, *333*, 58–65. [[CrossRef](#)]
46. Rosas, J.M.; Bedia, J.; Rodríguez-Mirasol, J.; Cordero, T. HEMP-derived activated carbon fibers by chemical activation with phosphoric acid. *Fuel* **2009**, *88*, 19–26. [[CrossRef](#)]
47. Sevilla, M.; Ferrero, G.A.; Fuertes, A.B. Beyond KOH activation for the synthesis of superactivated carbons from hydrochar. *Carbon N. Y.* **2017**, *114*, 50–58. [[CrossRef](#)]
48. Dubinin, M.M. Fundamentals of the theory of adsorption in micropores of carbon adsorbents: Characteristics of their adsorption properties and microporous structures. *Carbon* **1989**, *27*, 457–467. [[CrossRef](#)]
49. Rey, A.; Zazo, J.A.; Casas, J.A.; Bahamonde, A.; Rodriguez, J.J. Influence of the structural and surface characteristics of activated carbon on the catalytic decomposition of hydrogen peroxide. *Appl. Catal. A: Gen.* **2011**, *402*, 146–155. [[CrossRef](#)]
50. Sabio, E.; Álvarez-Murillo, A.; Román, S.; Ledesma, B. Conversion of tomato-peel waste into solid fuel by hydrothermal carbonization: Influence of the processing variables. *Waste Manag.* **2016**, *47*, 122–132. [[CrossRef](#)]
51. Falco, C.; Baccile, N.; Titirici, M.M. Morphological and structural differences between glucose, cellulose and lignocellulosic biomass derived hydrothermal carbons. *Green Chem.* **2011**, *13*, 3273–3281. [[CrossRef](#)]
52. Benstoem, F.; Becker, G.; Firk, J.; Kaless, M.; Wuest, D.; Pinnekamp, J.; Kruse, A. Elimination of micropollutants by activated carbon produced from fibers taken from wastewater screenings using hydrothermal carbonization. *J. Environ. Manag.* **2018**, *211*, 278–286. [[CrossRef](#)]
53. Sevilla, M.; Fuertes, A.B. The production of carbon materials by hydrothermal carbonization of cellulose. *Carbon N. Y.* **2009**, *47*, 2281–2289. [[CrossRef](#)]
54. Jian, X.; Zhuang, X.; Li, B.; Xu, X.; Wei, Z.; Song, Y.; Jiang, E. Comparison of characterization and adsorption of biochars produced from hydrothermal carbonization and pyrolysis. *Environ. Technol. Innov.* **2018**, *10*, 27–35. [[CrossRef](#)]
55. Mena, I.F.; Diaz, E.; Moreno-Andrade, I.; Rodriguez, J.J.; Mohedano, A.F. Stability of carbon-supported iron catalysts for catalytic wet peroxide oxidation of ionic liquids. *J. Environ. Chem. Eng.* **2018**, *6*, 6444–6450. [[CrossRef](#)]
56. Sevilla, M.; Maciá-Agulló, J.A.; Fuertes, A.B. Hydrothermal carbonization of biomass as a route for the sequestration of CO₂: Chemical and structural properties of the carbonized products. *Biomass Bioenerg.* **2011**, *35*, 3152–3159. [[CrossRef](#)]
57. Wang, T.; Zhai, Y.; Zhu, Y.; Li, C.; Zeng, G. A review of the hydrothermal carbonization of biomass waste for hydrochar formation: Process conditions, fundamentals, and physicochemical properties. *Renew. Sustain. Energy Rev.* **2018**, *90*, 223–247. [[CrossRef](#)]

58. He, C.; Zhao, J.; Yang, Y.; Wang, J.-Y. Multiscale characteristics dynamics of hydrochar from hydrothermal conversion of sewage sludge under sub- and near-critical water. *Bioresour. Technol.* **2016**, *211*, 486–493. [[CrossRef](#)]
59. Laginhas, C.; Nabais, J.M.V.; Titirici, M.M. Activated carbons with high nitrogen content by a combination of hydrothermal carbonization with activation. *Microporous Mesoporous Mater.* **2016**, *226*, 125–132. [[CrossRef](#)]
60. Rodríguez Correa, C.; Stollovsky, M.; Hehr, T.; Rauscher, Y.; Rolli, B.; Kruse, A. Influence of the carbonization process on activated carbon properties from lignin and lignin-rich biomasses. *ACS Sustain. Chem. Eng.* **2017**, *5*, 8222–8233. [[CrossRef](#)]
61. Figueiredo, J.L.; Pereira, M.F.R.; Freitas, M.M.A.; Órfao, J.J.M. Modification of the surface chemistry of activated carbons. *Carbon* **1999**, *37*, 1379–1389. [[CrossRef](#)]
62. Rey, A.; Hungria, A.B.; Duran-Valle, C.J.; Faraldos, M.; Bahamonde, A.; Casas, J.A.; Rodriguez, J.J. On the optimization of activated carbon-supported iron catalysts in catalytic peroxide oxidation process. *Appl. Catal. Environ. B.* **2016**, *181*, 249–259. [[CrossRef](#)]
63. Çalışkan, E.; Göktürk, S. Adsorption characteristics of sulfamethoxazole and metronidazole on activated carbon. *Sep. Sci. Technol.* **2010**, *45*, 244–255. [[CrossRef](#)]
64. Bajpai, A.K.; Rajpoot, M.; Mishra, D.D. Studies on the correlation between structure and adsorption of sulfonamide compounds. *Colloids Surf. A Physicochem. Eng. Asp.* **2000**, *168*, 193–205. [[CrossRef](#)]
65. Tonucci, M.C.; Gurgel, L.V.A.; de Aquino, S.F. Activated carbons from agricultural byproducts (pine tree and coconut shell), coal, and carbon nanotubes as adsorbents for removal of sulfamethoxazole from spiked aqueous solutions: Kinetic and thermodynamic studies. *Ind. Crops Prod.* **2015**, *74*, 111–121. [[CrossRef](#)]
66. Lu, X.; Berge, N.D. Influence of feedstock chemical composition on product formation and characteristics derived from the hydrothermal carbonization of mixed feedstocks. *Bioresour. Technol.* **2014**, *166*, 120–131. [[CrossRef](#)]
67. Rostamian, R.; Behnejad, H. A comparative adsorption study of sulfamethoxazole onto graphene and graphene oxide nanosheets through equilibrium, kinetic and thermodynamic modeling. *Process. Saf. Environ. Prot.* **2016**, *102*, 20–29. [[CrossRef](#)]



© 2019 by the authors. Licensee MDPI, Basel, Switzerland. This article is an open access article distributed under the terms and conditions of the Creative Commons Attribution (CC BY) license (<http://creativecommons.org/licenses/by/4.0/>).